CrossMark

RESEARCH PAPER

Role of polymer concentration and molecular weight on the rebounding behaviors of polymer solution droplet impacting on hydrophobic surfaces

Hyung Kyu Huh · Sungjune Jung · Kyung Won Seo · Sang Joon Lee

Abstract The impacting and rebounding behaviors of droplets containing polyethylene oxide (PEO) on Teflon-coated hydrophobic surface are investigated using a high-speed imaging system. Maximum spreading of droplets are examined experimentally by varying the concentration of polymer solution. During the spreading of droplets, no significant energy dissipation is found in the PEO solution droplets tested in this study. Energy dissipation during the retraction of contact line increases with the increase in the concentration and molecular weight of the polymer. Molecular weight does not show any noticeable effect when the concentration of the polymer solution is lower than 0.03 wt%. Its effect increases when the concentration is higher than 0.03 wt%, and the energy dissipation increases (threefold) at 0.05 wt% concentration. In addition, the residue composed of small satellite droplets is optically observed. The retraction velocity of contact line is decreased on the area of residue, which adds friction on the surface. A semiempirical model of energy balance equation is derived to estimate the rebounding tendency of a polymer solution droplet as a function of maximum spreading factor, retraction velocity, and reduced concentration. The
friction coefficient of the polymer solution shows a linear relationship with reduced concentration.

Keywords Drop impact · Rebounding behavior · Polymer solution droplet · Hydrophobic surface

1 Introduction

The impacting and spreading phenomena of droplets have been given much attention because of their significance in numerous engineering applications, such as spray coating (Aziz and Chandra 2000), spray cooling, surface cleaning, agricultural applications (Andrade et al. 2012a, b), and inkjet-printed electronic devices (Jung et al. 2013b; Lange et al. 2013; Secor et al. 2013). A substantial number of experimental studies have been conducted to understand the impacting and spreading behaviors of droplets based on their fluid properties (Fedorchenko et al. 2005; Jung and Hutchings 2012; Rioboo et al. 2002) or surface characteristics (Alizadeh et al. 2013; Antonini et al. 2013; Tran et al. 2013) by using high-speed imaging techniques.

Rioboo et al. (2002) classified the droplet impact phenomenon into five time-sequential phases: kinematic, spreading, relaxation, wetting, and equilibrium phases. Droplets exhibit different behaviors depending on surface wettability and their own physical properties. The impact phenomena of droplets can be divided into two different impact regimes, namely capillary and viscous regimes. The dimensionless Weber number ($We = \rho v_0^2 D_0/\sigma$) describes the relative importance of inertia and surface tension, whereas the Reynolds number ($Re = \rho v_0 D_0/\eta$) describes the relative importance of inertial force and viscous force on the impact of droplets. In these equations, ρ, v_0, D_0, σ,

H. K. Huh · K. W. Seo · S. J. Lee (✉)
Department of Mechanical Engineering, Center for Biofluid and Biomimic Research, Pohang University of Science and Technology, Pohang 790-784, Korea
e-mail: sjlee@postech.ac.kr

S. Jung
Department of Creative IT Engineering, Pohang University of Science and Technology, Pohang 790-784, Korea

and η indicate the density, initial velocity, initial diameter, surface tension, and viscosity of the working fluid, respectively. These numbers are essential in distinguishing the impact regime of droplets (Clanet et al. 2004). Maximum spreading factor ($\beta_{max} = D_{max}/D_0$) is an important parameter that describes the maximum extended state of droplets. D_{max} is the diameter of a droplet at the end of its spreading phase. Various theoretical and semiempirical models have been proposed to predict the maximum spreading factor of droplets impacting on various surfaces (Eggers et al. 2010; Lee et al. 2014; Roisman et al. 2002; Ukiwe and Kwok 2005). An and Lee (2012) investigated the maximum spreading factor of a shear-thinning liquid droplet impacted on a solid surface. According to high shear rate induced during the spreading and retracting phases, the viscosity of polymer solution decreases, which results in the decrease of energy dissipation (maximum spreading factor is reduced). Although understanding the underlying basic physics of the impact and spreading phases of a droplet is important, the final deposition of droplets on a substrate is significantly affected by the outcomes of the next phases.

In general, the impacting behaviors of droplets can be divided into six possible outcomes: deposition, prompt splash, corona splash, receding bread-up, partial rebound, and complete rebound (Rioboo et al. 2001). The rebounding phenomenon interrupts the fast and accurate deposition of droplets on hydrophobic surfaces. During the relaxation phase of a droplet that impacts on a hydrophobic surface, the elastic energy stored by the deformation of droplet retracts the contact line of the droplet. If the retraction speed is sufficient, then the droplet rebounds from the surface (Bergeron et al. 2000). One of the solutions to inhibit rebounding is to vary the surface tension of the working fluid by adding surfactants (MourougouCandoni et al. 1997). However, the addition of surfactant can also affect the formation of droplets by inducing undesirable problems such as generation of non-uniform droplet and splashing of droplet after impact.

Bergeron et al. (2000) first reported that as an alternative to surfactant additives, a small amount of polymer additives remarkably suppress the rebound of droplets without substantially affecting the bulk rheological properties of the working fluid. In their study, polyethylene oxide (PEO; 0.01 wt%, 4×10^6 g mol^{-1}) was added in the solution, and the droplet-retraction speed was gradually reduced. They claimed that the elongational viscosity induced by the elongation rate of impacting droplets is about three times higher than the shear viscosity of Newtonian fluid droplets, and it dissipates the initial kinetic energy more than the shear viscosity does, slowing down the droplet-retraction speed. However, other researchers asserted that the elongational viscosity does not significantly influence the spreading phase (Crooks et al. 2001; Rozhkov et al.

2003). The maximum spreading factors of droplets made of polymer solution and Newtonian fluids, as well as their diameter variations during the entire kinematic and spreading phases, are similar. This similarity cannot be explained fully by using the increased elongational viscosity (Bartolo et al. 2007; Jung et al. 2013a), since the viscous dissipation of energy should not only take place during the retracting phase, but it should also occur during the spreading phase. Alternatively, Bartolo et al. (2007) mentioned that the decrease in the retraction speed of polymer solution droplets is caused by non-Newtonian normal stresses. They added normal stresses to lubrication theory with capillarity and shear stresses to explain the decrease in droplet-retraction speed.

On the contrary, Bertola (2013) raised questions about non-Newtonian normal stresses for two reasons. First, the concentration of PEO solution used in their experiment was insufficiently diluted. In that case, the slow retraction is caused by high shear viscosity rather than normal stresses. Second, the normal stresses of the retracting contact line of dilute polymer solution droplet are insufficient to inhibit rebounding. Smith and Bertola (2010) observed that the stretched flexible polymer chains of λ-DNA or PEO chains remained behind the retracting contact line. They suggested that radially aligned chains of λ-DNA work as additional resistance to the contact line, which induces anti-rebound effect, thereby reducing retraction speed. Diluted polymer solution droplets impacting on heated substrates in the Leidenfrost regime do not form contact with the substrates, and therefore, they rebound from the surfaces (Bertola 2014). This indicates that the contact of a droplet of polymer solution and the substrate surface is important rather than non-Newtonian fluid-dynamic parameters. Therefore, current study focused on the importance of the reaction between polymer chains and surface. Smith and Sharp (2014) proved this importance by forced de-wetting of water and dilute PEO solution via a syringe-driven flow. They found that the additional contact-line friction caused by the presence of residual polymers increases with the increase in retraction speed.

However, the controversial roles of polymers on the anti-rebound effect still need further investigation to determine the origin of the additional friction force. In addition, the effects of polymer concentration and molecular weight should be quantitatively determined to understand the roles of polymers. In this study, the effects of polymer concentration and molecular weight on the anti-rebound effect are experimentally investigated. The optical evidence of residual polymers is directly observed using a high-speed camera. A semiempirical model accounting the contact-line friction according to polymer additives is suggested to estimate the rebounding phenomenon of polymer solution droplets.

2 Materials and experimental methods

PEO (Sigma-Aldrich) with molecular weights of 4×10^6 and 8×10^6 g mol^{-1} (designated as 4 M PEO and 8 M PEO, respectively) were dispersed in deionized water to concentrations of 0.0001–0.01 wt%, which corresponds to 1–100 ppm. The polymer solutions were stirred for 2 h at 40 °C constant temperature. When the concentration is higher than a critical concentration (c^*), polymer chains begin to interact with one another. The critical concentration of a dilute polymer solution can be estimated using the following equation (Clasen et al. 2006):

$$c^* = \frac{0.77}{[\eta]} \tag{1}$$

where $[\eta]$ is the intrinsic viscosity of the dilute polymer solution. Based on Zimm theory (Bremond and Villermaux 2006), $[\eta]$ is proportional to molecular weight and solvent quality. The intrinsic viscosity of dilute polymer solution is calculated using the following Mark–Houwink–Sakurada equation with coefficients 0.0125 and 0.78 for PEO solution in water (Bertola 2013):

$$[\eta] = 0.0125 M_w^{0.78} \; (\text{cm}^{-3}\,\text{g}^{-1}) \tag{2}$$

The critical concentrations calculated using Eqs. 1 and 2 are 0.0436 wt% for 4 M PEO and 0.0254 wt% for 8 M PEO solutions. Therefore, the highly concentrated 8 M PEO solution tested in this experiment exhibits a dilute regime and has polymer chains that are randomly coiled and dispersed without self-interaction. In general, polymer chains are elongated when shear rate is applied during the spreading and retraction phases of the droplet. The shear rate of a spreading droplet can be calculated by dividing the retraction velocity with the height variation of the droplet. In this experiment, the maximum shear rate of the impacting droplet is 8,400 s^{-1} when the impact velocity is 2.7 m/s. This indicates that polymer chains are fully stretched during the spreading and receding phases. The surface tension of water and the 8 M polymer solution measured by sessile drop method are 71.5 and 67 mN m^{-1}, respectively. The density ($\rho \approx 1.02$ g cm^{-3}) and viscosity ($\eta \approx 1.3$ mPa·s) of the 0.01 wt% 8 M PEO solution were measured using an electric balance with micropipetting and a viscometer (LVDV2+Pro, Brookfield), respectively. Given the low concentration of the

polymer additives, the surface tension, density, and viscosity of the polymer solution at varying polymer concentrations exhibit almost negligible differences within the range of experimental errors. Shear-thinning behavior of the PEO suspension is not observed under present experimental condition, because the zero shear viscosity and infinite shear viscosity are very similar. Table 1 compares the physical properties of polymer solutions tested in this study. Since the viscoelastic characteristics of polymer solutions do not show dominant energy dissipation in the spreading or retracing phase, direct measurement of viscosity according to shear rate or elasticity of PEO solution was not taken in this study. Those parameters are available in previous literatures (Christanti and Walker 2002; Tirtaatmadja et al. 2006). A glass slide (Superfrost-20, Matsunami) was cleaned with acetone and methanol to remove contaminants on the surface and then washed with distilled water. Teflon (Teflon amorphous fluoroplastic, Dupont) was diluted to 17 % with Fluorinert (FC-40, Sigma-Aldrich) and then coated on the clean glass using a spin coater (ACE-1020s, Dong Ah) to obtain a hydrophobic surface. Figure 1 shows the equilibrium state of water (a) and 0.01 wt% 4 M PEO solution (b) on the Teflon-coated surface. The equilibrium contact angle (θ_{eq}) of water droplets measured with a goniometer (SmartDrop, Femtofab Inc.) is 121° with a contact angle hysteresis (θ_h) of 8°. The corresponding values for 4 M PEO solution droplets are $\theta_{eq} \approx 106°$ with $\theta_h \approx 10°$.

The optical setup used to visualize droplet impact behaviors is depicted in Fig. 2. The impacting and rebounding behaviors of droplets were consecutively captured with a CMOS high-speed camera (Fastcam SA1.1, Photron) at 2,000 fps, which corresponds to a time interval of 0.5 ms. A macro zoom lens (Nikon AF Micro-Nikkor 60 mm) was attached in front of the camera. A metal halide lamp (MH-100, Dolan–Jenner) attached with an optical diffuser was used as light source, which was aligned with the lens and the camera. Each droplet was generated using a syringe pump and a needle with gauge number 27 (0.21 mm inner diameter). The vertical height between the impingement surface and the needle tip was adjusted to vary the impact velocity ($v_0 = 0.2$–2.7 m/s) of each droplet. The initial diameter of droplets, measured by counting the number of pixels and averaging them for 7–20 sequential images, is 3.25 ± 0.02 mm.

Table 1 Physical properties of the solutions tested in this study	4/8 M	0 wt%	0.0001 wt%	0.001 wt%	0.003 wt%	0.005 wt%
	γ (mN m^{-1})	71.5	70	68.2/67	68.2/67	68/67
	μ (mPa s)	1.28	1.28	1.28/1.29	1.28/1.29	1.28/1.3
	ρ (g cm^{-3})	1.02	0.12	1.02/1.01	1.02	1.02

Fig. 1 Droplets at equilibrium state lying on the Teflon-coated surface. **a** A water droplet with equilibrium contact angle of $\theta_{eq} = 121°$ and contact angle hysteresis of $\theta_h = 8°$. **b** A droplet of 0.01 wt% 4 M PEO with $\theta_{eq} = 106°$ and $\theta_h = 10°$
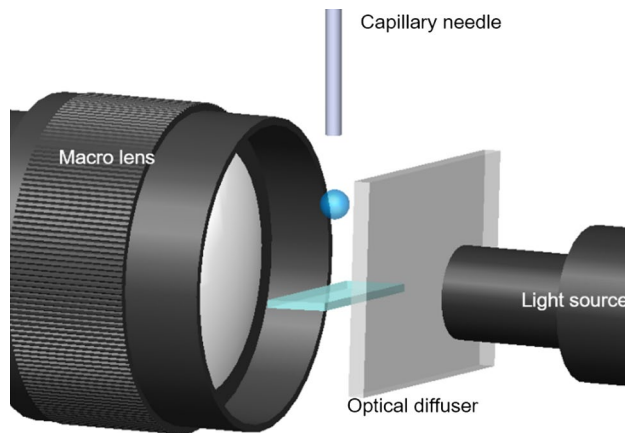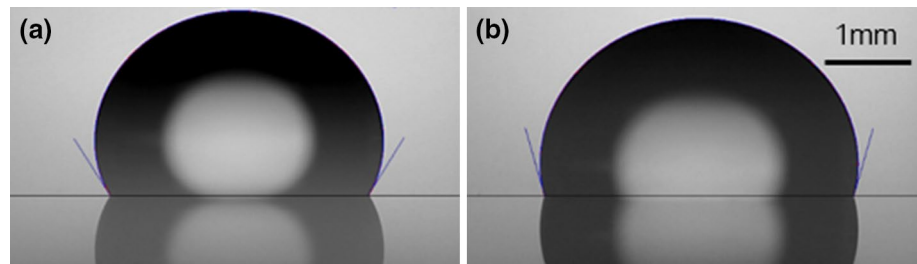

Fig. 2 Schematic diagram of the experimental setup composed of a macro zoom lens, a capillary needle, an optical diffuser, and a light source

3 Results and discussion

3.1 Impact regimes and maximum spreading of droplets

Figure 3 shows the impact regimes of water droplet and droplets of 4 M PEO solutions with concentrations of 0.0001, 0.001, and 0.01 wt% based on We and Re. The dotted line in the figure represents the case of impact number ($P = We/\text{Re}^{4/5}$) of 1 for the given dimensionless numbers; P distinguishes the dominant energy dissipation mechanisms of an impacting droplet (Clanet et al. 2004). In the capillary regime ($P < 1$), the initial kinetic energy of droplets is mostly converted into surface energy. On the contrary, viscous energy dissipation is dominant in the viscous regime ($P > 1$). Results showed that all droplets with different concentrations and initial impact velocity exhibit the capillary regime (Fig. 3). Thus, the conversion of initial kinetic energy of each droplet into surface energy is more dominant than viscous dissipation.

The maximum spreading factors of water and 4 M PEO droplets increase relative to We, as shown in Fig. 4. Interestingly, all of the data fall in a single curve, independent of polymer concentration. They follow the scaling law of $\beta_{max} \sim \text{We}^{1/4}$ (dashed line) for We larger than 20. This result implies that the impact phenomenon belongs to the capillary regime, and the initial kinetic energy of droplets is
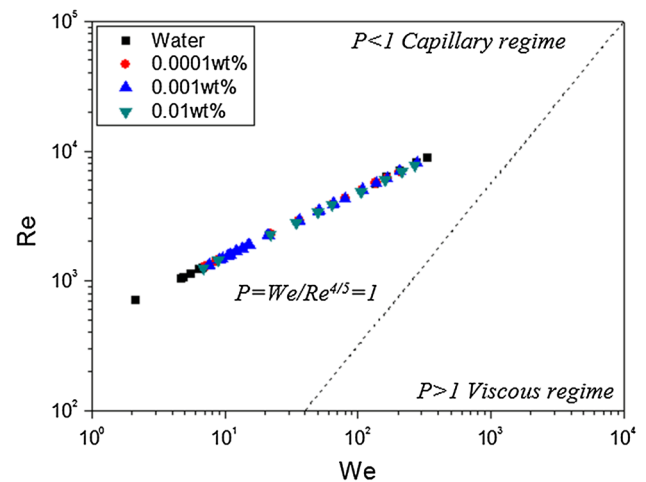

Fig. 3 Impact regimes for water droplet (*filled square*) and 4 M PEO droplets with concentration of 0.0001 (*filled circle*), 0.001 (*filled triangle*), and 0.01 (*filled inverted triangle*) wt%. Dashed line indicates the case of impact number $P = 1$. All the impacting droplets tested in this experiment belongs to the capillary regime
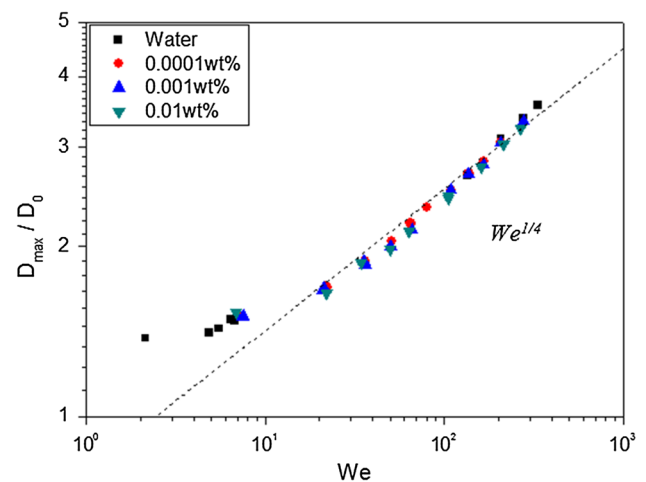

Fig. 4 The maximum spreading factors of water droplets (*filled square*) and 4 M PEO droplets with concentration of 0.0001 (*filled circle*), 0.001 (*filled triangle*), and 0.01 (*filled inverted triangle*) wt% on the Teflon-coated surface. *Dashed line* denotes the scaling law of $\beta \sim \text{We}^{1/4}$

Fig. 5 Oscillation phenomena of impact droplets. **a** Gentle bouncing of water and anti-rebound of 4 M PEO droplets with polymer concentration of **b** 0.0001, **c** 0.001, **d** 0.01 wt% on Teflon-coated surface at Weber number of 7. **e** 0.0001 and **f** 0.01 wt% 4 M PEO droplets impacted at Weber number of 105 show vigorous bouncing and anti-rebound, respectively. *Solid arrow* indicates polymer residue after contact-line retraction, and *horizontal dotted arrows* indicate the maximum spreading factor
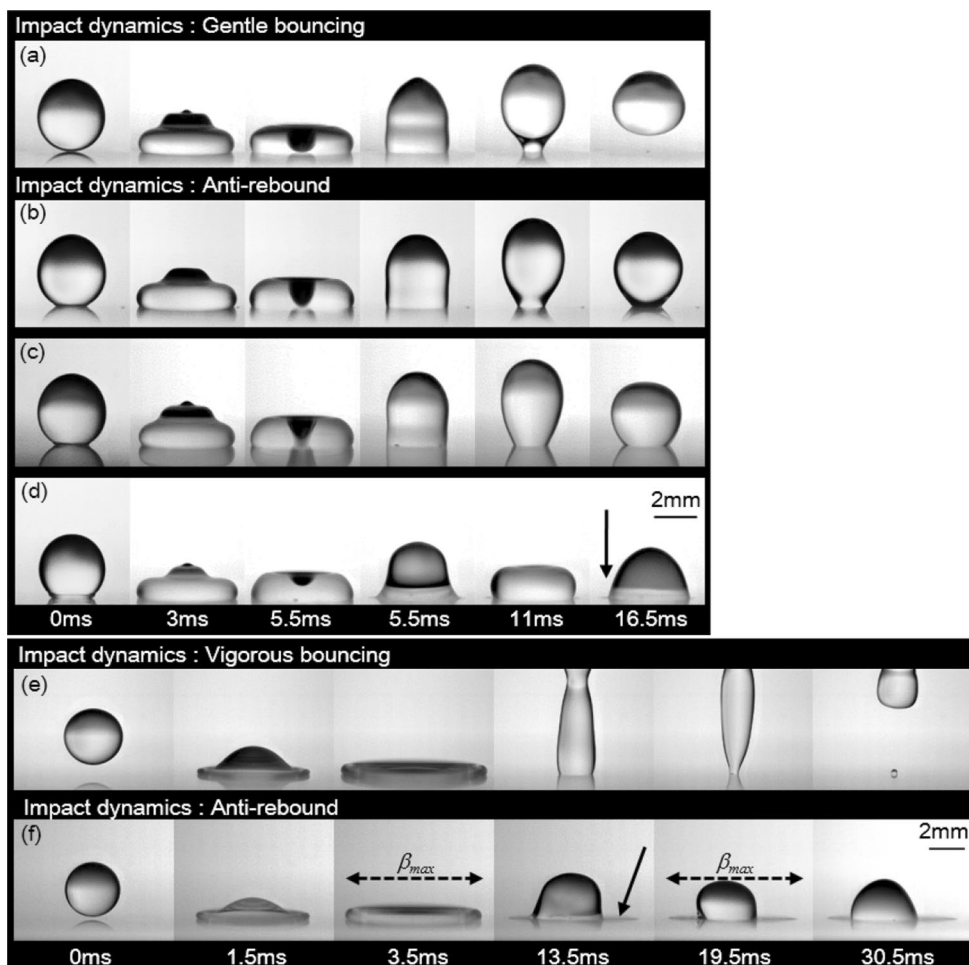
transformed into surface energy until the droplets reach their maximum spreading state (Clanet et al. 2004), which matches well with the result shown in Fig. 3. It is also a counterevidence of the hypothesis that the increased elongational viscosity dissipates initial kinetic energy, since there is no significant energy dissipation during the spreading phase, regardless of polymer concentration. For PEO in water with molecular weight over 4 M g mol^{-1}, the maximum spreading factor is a universal function of We, regardless of polymer concentration (when it is smaller than 0.01 wt%). However, as the concentration of the polymer solution increases, its viscosity is also increased. Therefore, the viscous dissipation has to be considered along with the surface energy. When the concentration of the polymer solution is higher than 0.01 wt%, the maximum spreading factor β_{max} is reduced due to the additional energy dissipation by viscosity. Therefore, it does not follow the scaling law of $\beta_{max} \sim We^{1/4}$ any longer.

3.2 Effect of polymer concentration

Temporal evolution of impact behavior of droplets on the Teflon-coated surface was sequentially recorded to investigate the effects of polymer concentration and impact velocity on the impacting phenomenon. Figure 5a–d shows the impacting behavior of water, 0.0001, 0.001, and 0.01 wt% 4 M PEO solution droplets at relatively low impact velocity ($v_0 = 0.4$ m s^{-1}, We $= 7$). Figure 5e, f shows the impact process of 0.0001 and 0.01 wt% 4 M PEO droplets at higher velocity ($v_0 = 1.56$ m s^{-1}, We $= 105$).

Impact dynamics can be categorized into gentle, vigorous bouncing, and anti-rebound depending on rebound height and droplet shape. Figure 5a displays a typical case of gentle bouncing, for which a droplet is detached right above the surface while maintaining its spherical shape. If the droplet does not have sufficient kinetic energy to overcome the energy dissipation during the spreading and retraction of contact line, then it is not detached from the surface (Fig. 5b–d, f). Droplets of polymer additives leave residue whose diameter is similar to the maximum spreading diameter (dashed arrow) after contact line is retracted (solid arrow). Polymer residue is clearly observed as the polymer concentration increases. The effect of polymer residue is discussed in Sect. 3.4. Vigorous bouncing occurs

when the initial kinetic energy is sufficient to rebound droplets in an elongated shape (Fig. 5e).

Although the effect of polymer additives on the maximum spreading factor is negligible, the influence of the polymer addition is significant during the retraction phase. As the polymer concentration increases, the contact-line diameter of a retracting droplet at a low impact velocity increases, which implies that the contact-line velocity is reduced. Therefore, gentle bouncing of water droplets occurs when $v_0 = 0.4$ m s^{-1}, whereas PEO droplets show anti-rebound behaviors. However, the addition of polymers cannot suppress the rebound of droplets when the impact velocity, that is, the initial kinetic energy, is sufficiently high.

Figure 6 shows temporal variation of contact-line diameter from which the role of polymer concentration can be quantitatively understood. Figure 6a corresponds to the images in Fig. 5a–d when the impact velocity is $v_0 = 0.4$ m s^{-1} for water and 4 M PEO droplets. The normalized contact-line diameter (D_b/D_0) of each droplet increases in the spreading phase according to the dimensionless time ($\tau = tv_0/D_0$) until it reaches the maximum contact-line spreading factor ($\beta_{c,\max}$), which is marked by the dashed arrow. Here, D_b indicates contact-line diameter. The contact-line diameters of PEO droplets with different concentrations do not show noticeable difference during the spreading phase. However, the contact-line speed is reduced during the retraction phase as the polymer concentration increases. In addition, the oscillating contact-line diameter in the relaxation phase is suppressed, as indicated by the solid arrow in Fig. 6a. Although the viscoelastic behavior of polymer solution increases according to the concentration of the solution, the PEO suspension used in this experiment is extremely diluted. In addition, the elastic behavior reduces the frequency of vertical oscillation during the relaxation phase (Son and Kim 2009). Therefore, the decrease of retraction speed and the suppression of contact-line oscillation amplitude can be explained mainly by the additional energy dissipation caused by polymer additives.

Figure 6b shows variations of the normalized contact-line diameter of impacting droplets with different concentrations of polymer additives on the Teflon-coated surface with $v_0 = 1.56$ m s^{-1}. The maximum spreading factor $\beta_{c,\max}$ of the contact-line diameter in Fig. 6b is larger than that at low impact velocity (Fig. 6a), regardless of polymer concentration. Polymer concentration does not have strong influence on the duration time of the spreading phase. However, the retraction and relaxation phases are extended as the polymer concentration increases, as marked with the solid arrow in Fig. 6b. Although the addition of polymer decreases the retraction velocities, vigorous bouncing occurs (Fig. 5e) because of sufficient initial kinetic energy
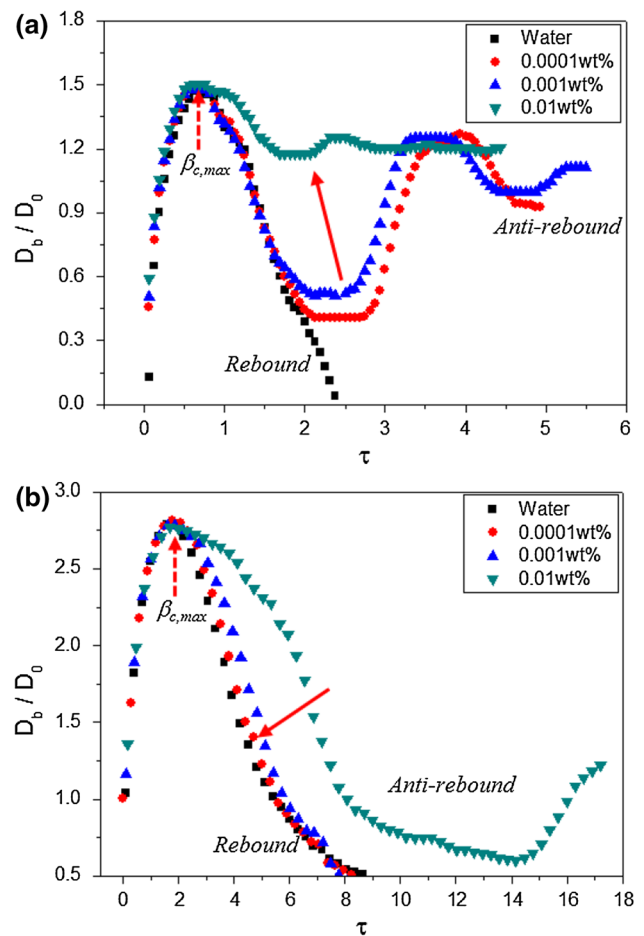

Fig. 6 Temporal variations of normalized contact-line diameter according to the dimensionless time. (*filled square*), (*filled circle*), (*filled triangle*), and (*filled inverted triangle*) indicate diameters of water, 0.0001, 0.001, and 0.01 wt% concentrated 4 M PEO droplets, respectively. *Dashed arrow* indicates the normalized maximum contact-line diameter. **a** Normalized diameter of impact droplets on the Teflon-coated surface at Weber number of 7. *Solid arrow* denotes reduction of contact-line oscillation and retraction velocity. **b** Droplets impacted on the Teflon-coated surface at Weber number of 165. *Solid arrow* indicates the increase of contact-line velocity, as the polymer concentration decreases

except for the case of 0.01 wt% concentrated 4 M PEO solution.

3.3 Effect of polymer molecular weight

Figure 7 shows the impact phenomena of droplets of equally concentrated (a, b: 0.003 wt%; and c, d: 0.005 wt%) PEO solution with different molecular weights (a, c: 4 M; and b, d: 8 M) on the Teflon-coated surface at low and high initial impact velocities ($v_0 = 0.78$ m s^{-1}, We = 28 for a, b; and $v_0 = 1.55$ m s^{-1}, We = 105 for c, d). The figure displays the role of polymer molecular weight on the rebound of PEO droplets. Polymer solution at low concentration

Fig. 7 Impact dynamics of PEO droplets on the Teflon-coated surface. **a** 0.003 wt% 4 M PEO droplet and **b** 8 M PEO droplet gently bounces from the surface when Weber number is 28. **c** 0.005 wt% 4 M PEO droplet gently bounces, while (**d**) 8 M PEO droplet sticks to the surface, i.e., anti-rebounds when Weber number is 105. *Solid arrow* indicates polymer residue after retraction of contact line. *Horizontal arrows* denote the maximum spreading factor
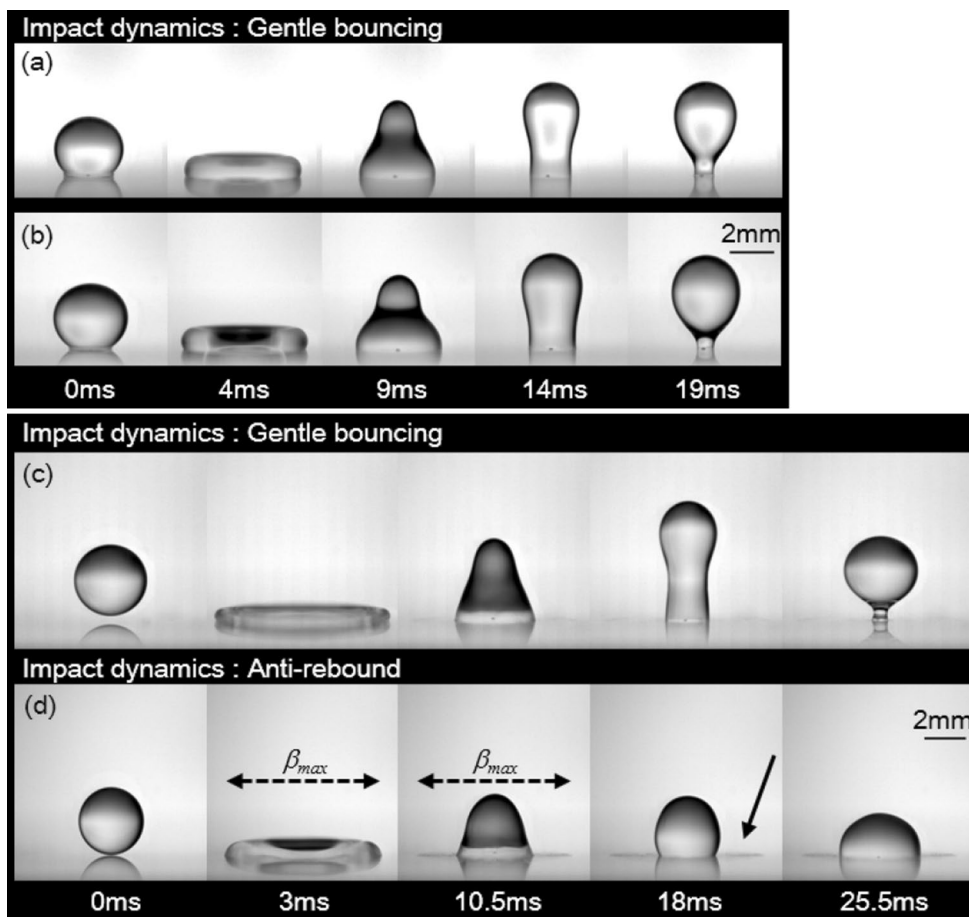
(0.003 wt%) shows gentle bouncing of droplets, regardless of polymer molecular weight (Fig. 7a, b). However, high polymer concentration (0.005 wt%) prohibits the rebound of droplet as the molecular weight increases. 4 M PEO droplets gently bounce from the surface when $v_0 = 1.55$ m s^{-1}, whereas the rebound of 8 M PEO droplets is suppressed at the same impact velocity (Fig. 7c, d). Polymer residue is observed when the concentration of 8 M polymer solution is higher than 0.005 wt%, as indicated by the solid arrow in Fig. 7d. The size of residue is nearly similar to the maximum spreading diameter. The effect of polymer molecular weight on the anti-rebound of droplets is different for 4 and 8 M PEO solutions at 0.003 wt% concentration.

Temporal variations of the normalized contact-line diameters of 0.003 and 0.005 wt% concentrated 4 and 8 M PEO droplets are compared to quantify the effect of molecular weight at two different impact velocities. The normalized contact-line diameters are clearly indistinguishable during the entire spreading and retraction phases at the same impact velocity (Fig. 8). The maximum spreading factors are unnoticeably influenced by polymer molecular weight because of the diluted concentration of the polymer solutions. The contact time of droplets on the hydrophobic
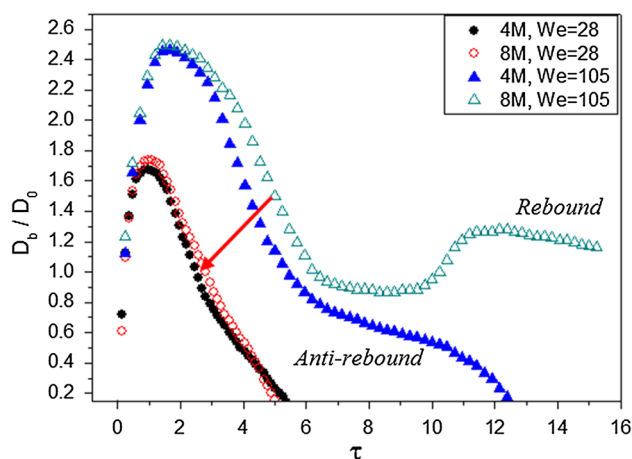

Fig. 8 Temporal variation of the normalized diameter of 0.003 wt% 4 M PEO droplets (*filled circle*) and 8 M PEO droplets (*open circle*) impacted on the Teflon-coated surface at Weber number of 28. The symbols (*filled triangle*) and (*open triangle*) indicate the impact droplets of 0.005 wt% 4 M PEO solution and 8 M PEO solution at Weber number of 105. *Solid arrow* indicates that the dimensionless contact time decreases as Weber number increases

surface decreases with the increase in polymer molecular weight and impact velocity, as indicated by the solid arrow. The effect of polymer molecular weight, that is, polymer

chain length, on the suppression of droplet rebound is closely related with polymer concentration. These factors should not be handled independently in the estimation of anti-rebound phenomenon of PEO droplets. The effect of molecular weight on the polymer solution is diminished, when the concentration of the polymer solution is normalized by the critical concentration c^*. The critical concentration contains the information about the molecular weight as expressed in Eq. 1. This will be further discussed in the Sect. 3.5.

3.4 Effect of polymer residue

As shown in Figs. 5d and 7d, polymer residue remained after the retraction of contact line. However, this residue is no longer detectable with the use of an optical imaging system after a certain period. This result implies that the polymer residue is mostly composed of small-sized droplets of the solution. One possible hypothesis is the formation of beads-on-a-string (BOAS) structures during the retraction process. When the polymer-containing filaments are stretched, BOAS structures are formed in the case of break up (Bhat et al. 2010). In the same manner, PEO starts to interact adhesively with the Teflon-coated surface during the retraction of contact line, when the inertia force pulls the contact line inward. In stretching the working fluid, small satellite beads are formed. However, to understand the origin of adhesion forces between polymer chains and the surface, detailed analysis on the interaction between polymer surface and working fluid is required. The present study focuses on the effects of polymer concentration and molecular weight on the additional energy dissipation, rather than revealing the origin of the adhesive forces.

A two-step experiment was conducted to determine the role of polymer residue on the anti-rebound behavior of PEO droplets. At first, a droplet of 0.05 wt% concentrated 4 M PEO solution was impacted on the Teflon-coated surface. The residue area of polymer residue around the primary droplet is indicated with the horizontal dashed-dot arrow in Fig. 9 by tracking the maximum spreading factor. Droplets with the same concentration and molecular weight are then impacted on the Teflon surface at the position just next to the impact point of previous droplet to overlap the residue area of each droplet. The retraction speed of contact line of the second droplet on the overlapped area (left) is reduced to half of the non-residue area (right) (marked with solid and dashed arrows in Fig. 9, respectively). The pixel intensity of the overlapped residue area is increased compared with that of the non-residue side. This finding suggests that more satellites are formed during the retraction phase. The second droplet rebounds toward the first droplet because of the difference in retraction velocities of the
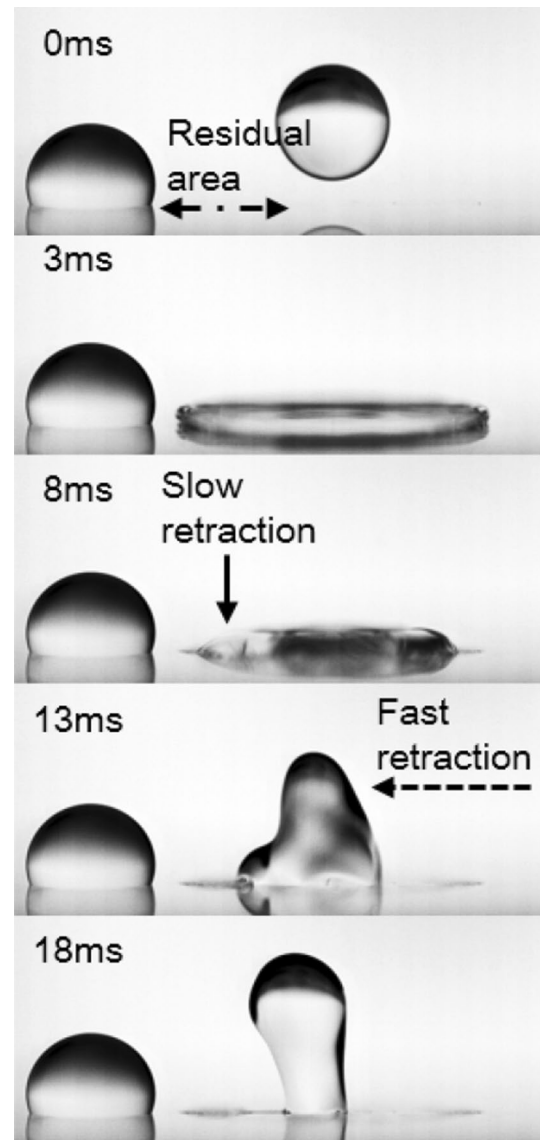

Fig. 9 The role of polymer residue on the anti-rebound behavior of 0.05 wt% 4 M PEO droplets. Primary droplet (*left*) is impacted on the Teflon-coated surface. *Dashed-dot arrow* indicates residue area around the primary droplet. Secondary droplet (*right*) is impacted on the residue area of the first droplet. Retraction contact-line speed of the overlapped area (*solid arrow*) is slower than that of the original hydrophobic surface (*dashed arrow*)

left and right sides (see Movie S1). These results imply that the polymer residue contributes dominantly to the dissipation of initial kinetic energy of droplets and suppresses the rebound phenomenon.

3.5 Theoretical analysis

Figure 10a shows variations of critical We (We*) according to the polymer concentration of 4 M and 8 M PEO solution droplets. We* is defined as the We at which
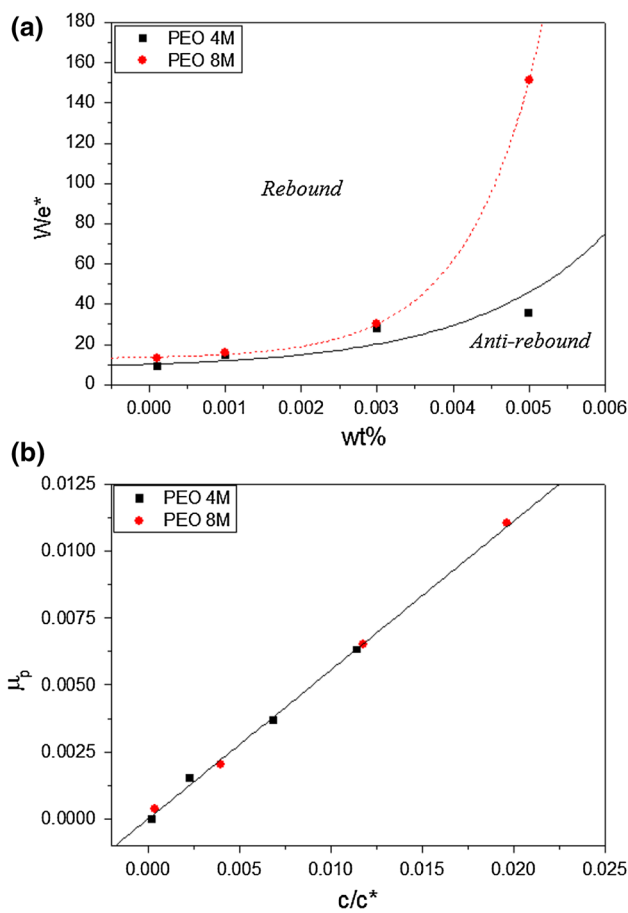
Fig. 10 a Variations of the critical Weber number for 4 M (*filled square*) and 8 M (*filled circle*) PEO droplets according to the polymer concentration. *Dashed line* and *solid line* represent the first-order exponential decay curve fittings of 4 and 8 M PEO solution droplets, respectively. **b** Variation of friction factor induced by polymer additives with respect to the reduced concentration. *Solid line* indicates a liner relationship with a slope of 0.55

droplet starts to rebound from the substrate (gentle rebound). The fitting curve of each solution, dashed line (8 M) and solid line (4 M), displays the first-order exponential decay. We* increases as the polymer concentration increases. The values of both polymer solutions are overlapped when the concentration is smaller than 0.003 wt%. This result indicates that molecular weight does not affect extremely diluted polymer solution. The We* of 8 M PEO solution is almost three times that of 4 M PEO solution when the polymer concentration is 0.005 wt%. The effect of molecular weight increases as the concentration increases.

The rebound phenomenon of droplets can be estimated by using the energy-balanced semiempirical model suggested by Mao et al. (1997). Rebound occurs when the normalized droplet excess rebound energy has a positive value ($E^*_{ERE} > 0$). The droplet excess rebound energy is

a function of the maximum spreading factor and Young's contact angle (Eq. 3)

$$E^*_{ERE} = \frac{1}{4}\beta^2_{max}(1 - \cos\theta_{eq}) - 0.12\beta^{2.3}(1 - \cos\theta_{eq})^{0.63}$$
$$+ \frac{2}{3\beta_{max}} - 1 \tag{3}$$

However, the rebound behaviors of polymer solution cannot be estimated by Eq. 3 because of the additional energy dissipation by polymer additives. Therefore, the additional energy dissipation during the retraction phase must be considered in the energy balance model to obtain accurate prediction of the rebound phenomena of PEO droplets. All energy terms and the overall energy balance for a PEO droplet are discussed below.

Since the impact regime of a droplet belongs to the capillary regime, viscous dissipation during the spreading phase is negligible, as mentioned in Sect. 3.1. In addition, because the contact line is driven by inertia in the spreading phase, an energy balance model can be established from the maximum spreading state of the droplet. A droplet at the maximum spreading state is assumed as a thin circular disk. Although this assumption is somewhat unrealistic, yet the models derived based on this assumption are robust and the theoretical analysis on the dynamic behaviors of a droplet shows good agreement with experimental results (German and Bertola 2009; Healy et al. 2001; Mao et al. 1997; Ukiwe and Kwok 2005). The top surface area, the circumferential edge area, and the height of the disk are expressed as $(\pi/4)D^2_{max}$, $2\pi/3(D^3_0/D_{max})$ and $2/3(D^3_0 D^2_{max})$, respectively. The contact line of the droplet is momentarily paused at the maximum spreading state, and the kinetic energy becomes zero. Therefore, the surface energy of the circular disk represents the total energy, as follows:

$$E_{max} = \left[\frac{\pi}{4}D^2_{max}(1 - \cos\theta) + \frac{2\pi}{3}\frac{D^3}{D_{max}}\right]\sigma \tag{4}$$

Here, the surface tensions of liquid–air and liquid–solid are multiplied to the corresponding surface area of the disk. Using the Young's equation, the two different surface tensions are simplified into the liquid–air surface tension and the initial contact angle.

As suggested by Mao et al. (1997), the energy dissipation $E_{diss,rec}$ during the contact-line retraction can be estimated by the following empirical correlation as a function of the maximum spreading factor and Young's contact angle:

$$E_{diss,rec} = 0.12\beta^{2.3}_{max}(1 - \cos\theta_{eq})^{0.63}\pi D^2_0\sigma \tag{5}$$

The above equation was established based on the experimental data by the help of least-square data regression. It

contains the maximum spreading factor and the Young's contact angle. The dimension of the correlation is the same as the surface energy of a droplet.

During the contact line retraction of a polymer solution droplet, the additional energy dissipation by polymer additives $E_{\mathrm{diss},p}$ can be estimated by modifying the contact-line dissipation rate ($\dot{R}_{\mathrm{DG}} = 2\pi r \mu_f v_{cl}^2$), which was formulated by de Gennes (1985). This simple yet robust equation can be applied to various cases (inhomogeneous or rough surface, polymer residue, etc.) where the contact line of the droplet experiences additional resistance by friction force. Here, the contact-line dissipation rate is given as a function of the contact-line friction factor μ_f and contact-line velocity v_{cl}. The energy dissipation term modified by the addition of polymer additives can be described as:

$$E_{\mathrm{diss},p} = \pi D_{\max} \mu_p v_{\mathrm{rec}}^2 t_{\mathrm{rec}} \tag{6}$$

where μ_p is the friction factor induced by polymer additives. The retraction velocity v_{rec} and the receding time t_{rec} are experimentally measured. In this equation, the retraction velocity is obtained by dividing the displacement of contact line from the maximum spreading state to its original diameter by the receding time [$v_{\mathrm{rec}} = (D_{\max} - D_0)/t_{\mathrm{rec}}$]. Since the dimension of Eq. 6 is the same as the surface energy, it can be directly used in the energy balance equation to represent the energy dissipated by additional friction induced by the polymer residue.

When a droplet is gently bounced just above the surface with its original spherical shape, the final energy E_f of the droplet is only the surface energy of a spherical droplet:

$$E_f = \pi D_0^2 \sigma \tag{7}$$

The overall energy balance should satisfy the following relation when a droplet is gently rebounded from a flat substrate:

$$E_{\max} - E_{\mathrm{diss,rec}} - E_{\mathrm{diss},p} = E_f \tag{8}$$

The equation states the energy balance between the maximum spreading state and the final rebounded state of the droplet. Between the two states, energy is dissipated by the retraction itself and the polymer residue through the retraction phase. The energy dissipated by the polymer additives is the only unknown. It can be calculated by substituting the experimentally measured parameters to the other energy terms. The friction coefficient μ_p is calculated after $E_{\mathrm{diss},p}$ is driven from the energy balance equation which is a function of polymer concentration and molecular weight. The effect of polymer molecular weight can be diminished by using reduced concentration (c/c^*), as shown in Fig. 10b, where c is the concentration of the droplet solution. The curves of μ_p for 4 and 8 M PEO solutions fall into a single linear curve of $\mu_p \approx \alpha\,(c/c^*)$, where $\alpha = 0.55$ for PEO solution.
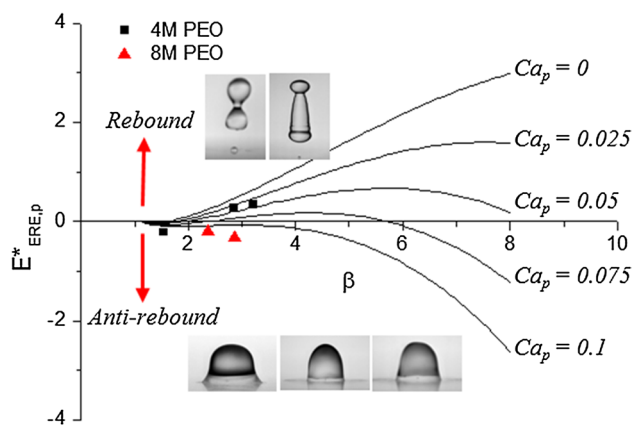

Fig. 11 Variations of the normalized droplet excess rebound energy of polymer solution estimated with Eq. 9 according to the maximum spreading factor at various capillary numbers Ca$_p$. $E_{\mathrm{ERE},p}^*$ calculated experimentally for 4 M (*filled square*) and 8 M (*filled circle*) polymer solution shows good agreement with the semiempirical estimation. *Inset* figures show rebound (*upper*) and anti-rebound phenomena (*below*)

The normalized excess rebound energy of PEO droplet ($E_{\mathrm{ERE},p}^*$) can be estimated by using the following semiempirical model, which substitutes Eq. 6 in Eq. 3:

$$E_{\mathrm{ERE},p}^* = \frac{1}{4}\beta_{\max}^2(1 - \cos\theta) - 0.12\beta_{\max}^{2.3}(1 - \cos\theta)^{0.63}$$
$$+ \frac{2}{3\beta_{\max}} - 1 - \mathrm{Ca}_p(\beta - 1)\beta \tag{9}$$

where $\mathrm{Ca}_p = \mu_p v_{\mathrm{rec}}/\sigma$ is a dimensionless capillary number of polymer droplet representing the relative effect of the polymer-induced resistance to the surface tension. PEO droplets gently rebound from the surface when $E_{\mathrm{ERE},p}^* = 0$.

Figure 11 shows the variations in $E_{\mathrm{ERE},p}^*$ of PEO solution with various Ca$_p$ according to the maximum spreading factor. The general tendency of droplet rebound is increased as the maximum spreading factor increases at low Ca$_p$ values. However, the trend of PEO droplet rebound is either increased or decreased with increasing Ca$_p$. The additional energy dissipation caused by polymer additives is increased as the area of polymer residue (that is, the maximum spreading factor) increases. This phenomenon is verified by experimental observations of PEO droplets with varying polymer concentrations and molecular weights. When a droplet of 4 M PEO solution with a concentration of 0.0001 and 0.01 rebounds from the substrate as shown in the upper inset image of Fig. 11, the corresponding experimentally calculated data points marked as rectangular symbol have positive sign. As the Ca$_p$ of the solution increases, the experimentally calculated $E_{\mathrm{ERE},p}^*$ starts to show negative sign and the rebounding phenomena are suppressed as depicted in the below inset image. This implies that the

semiempirical estimations are well matched with given the experimental data.

4 Conclusions

The impact and rebound behaviors of PEO droplets on Teflon-coated hydrophobic surface were experimentally investigated by varying the concentrations and molecular weights of the polymer solution. Energy dissipation caused by the addition of polymer additives in the spreading phase is not so significant when the maximum spreading factors for PEO droplets at different concentrations are compared. On the contrary, the effects of polymer concentration and molecular weight are considerable during the contact-line retraction of droplet. The tendency of droplet rebound is decreased with increase in the concentration and molecular weight of the polymer solution.

Polymer residue is optically observed after the contact-line retraction of PEO droplets. The polymer chains remained on the surface with small satellite droplets in the form of BOAS structure. The contact-line retraction velocity of droplets impacted on the residue area is smaller than that of the normal Teflon-coated surface. The residue area is nearly similar to the maximum spreading area; thus, the energy dissipation caused by the presence of polymer additives is a complex function of the concentration and molecular weight of polymer solution, the contact-line retraction velocity, and the area of polymer residue.

The friction factor of PEO droplets was estimated by using an energy balance equation. The friction factor shows a linear relationship with the reduced concentration, regardless of concentration and molecular weight of polymer solution. A semiempirical model was derived to estimate the rebound tendency of a PEO droplet, which is a function of the maximum spreading factor and capillary number of polymer solution. This study is beneficial for understanding the origin of contact-line friction of a polymer solution and the effects of its concentration and molecular weight on the anti-rebound of PEO droplets.

References

Alizadeh A, Bahadur V, Shang W, Zhu Y, Buckley D, Dhinojwala A, Sohal M (2013) Influence of substrate elasticity on droplet impact dynamics. Langmuir 29:4520–4524

An SM, Lee SY (2012) Maximum spreading of a shear-thinning liquid drop impacting on dry solid surfaces. Exp Therm Fluid Sci 38:140–148

Andrade R, Skurtys O, Osorio F (2012a) Experimental study of drop impacts and spreading on epicarps: effect of fluid properties. J Food Eng 109:430–437

Andrade RD, Skurtys O, Osorio F (2012b) The impact of liquid drops on purple cabbage leaves (Brassica oleracea l. Var. Capitata). Ing Invest 32:79–82

Antonini C, Bernagozzi I, Jung S, Poulikakos D, Marengo M (2013) Water drops dancing on ice: how sublimation leads to drop rebound. Phys Rev Lett 111:014501

Aziz SD, Chandra S (2000) Impact, recoil and splashing of molten metal droplets. Int J Heat Mass Tran 43:2841–2857

Bartolo D, Boudaoud A, Narcy G, Bonn D (2007) Dynamics of non-newtonian droplets. Phys Rev Lett 99:174502

Bergeron V, Bonn D, Martin JY, Vovelle L (2000) Controlling droplet deposition with polymer additives. Nature 405:772–775

Bertola V (2013) Dynamic wetting of dilute polymer solutions: the case of impacting droplets. Adv Colloid Interfac 193:1–11

Bertola V (2014) Effect of polymer concentration on the dynamics of dilute polymer solution drops impacting on heated surfaces in the Leidenfrost regime. Exp Therm Fluid Sci 52:259–269

Bhat PP, Appathurai S, Harris MT, Pasquali M, McKinley GH, Basaran OA (2010) Formation of beads-on-a-string structures during break-up of viscoelastic filaments. Nat Phys 6:625–631

Bremond N, Villermaux E (2006) Atomization by jet impact. J Fluid Mech 549:273–306

Christanti Y, Walker LM (2002) Effect of fluid relaxation time of dilute polymer solutions on jet breakup due to a forced disturbance. J Rheol 46:733–748

Clanet C, Beguin C, Richard D, Quere D (2004) Maximal deformation of an impacting drop. J Fluid Mech 517:199–208

Clasen C et al (2006) How dilute are dilute solutions in extensional flows? J Rheol 50:849–881

Crooks R, Cooper-Whitez J, Boger DV (2001) The role of dynamic surface tension and elasticity on the dynamics of drop impact. Chem Eng Sci 56:5575–5592

de Gennes PG (1985) Wetting: statics and dynamics. Rev Mod Phys 57:827–863

Eggers J, Fontelos MA, Josserand C, Zaleski S (2010) Drop dynamics after impact on a solid wall: theory and simulations. Phys Fluids 22:062101

Fedorchenko AI, Wang AB, Wang YH (2005) Effect of capillary and viscous forces on spreading of a liquid drop impinging on a solid surface. Phys Fluids 17:093104

German G, Bertola V (2009) Review of drop impact models and validation with high-viscosity Newtonian fluids. At Spray 19:787–807

Healy WM, Hartley JG, Abdel-Khalik SI (2001) Surface wetting effects on the spreading of liquid droplets impacting a solid surface at low Weber numbers. Int J Heat Mass Transf 44:235–240

Jung S, Hutchings IM (2012) The impact and spreading of a small liquid drop on a non-porous substrate over an extended time scale. Soft Matter 8:2686–2696

Jung SJ, Hoath SD, Hutchings IM (2013a) The role of viscoelasticity in drop impact and spreading for inkjet printing of polymer solution on a wettable surface. Microfluid Nanofluid 14:163–169

Jung SJ, Sou A, Gili E, Sirringhaus H (2013b) Inkjet-printed resistors with a wide resistance range for printed read-only memory applications. Org Electron 14:699–702

Lange A, Schindler W, Wegener M, Fostiropoulos K, Janietz S (2013) Inkjet printed solar cell active layers based on a novel, amorphous polymer. J Nanosci Nanotechnol 13:5209–5214

Lee SJ, Huh HK, Kwon DH (2014) Energy dissipation of graphene colloidal suspension droplets impacting on solid substrates. RSC Adv 4:7216–7224

Mao T, Kuhn DCS, Tran H (1997) Spread and rebound of liquid droplets upon impact on flat surfaces. AIChE J 43:2169–2179

MourougouCandoni N, PrunetFoch B, Legay F, VignesAdler M, Wong K (1997) Influence of dynamic surface tension on the spreading of surfactant solution droplets impacting onto a low-surface-energy solid substrate. J Colloid Interface Sci 192:129–141

Rioboo R, Tropea C, Marengo M (2001) Outcomes from a drop impact on solid surfaces. At Spray 11:155–165

Rioboo R, Marengo M, Tropea C (2002) Time evolution of liquid drop impact onto solid, dry surfaces. Exp Fluids 33:112–124

Roisman IV, Rioboo R, Tropea C (2002) Normal impact of a liquid drop on a dry surface: model for spreading and receding. Proc Roy Soc A Math Phys 458:1411–1430

Rozhkov A, Prunet-Foch B, Vignes-Adler M (2003) Impact of drops of polymer solutions on small targets. Phys Fluids 15:2006–2019

Secor EB, Prabhumirashi PL, Puntambekar K, Geier ML, Hersam MC (2013) Inkjet printing of high conductivity, flexible graphene patterns. J Phys Chem Lett 4:1347–1351

Smith MI, Bertola V (2010) Effect of polymer additives on the wetting of impacting droplets. Phys Rev Lett 104:154502

Smith MI, Sharp JS (2014) Origin of contact line forces during the retraction of dilute polymer solution drops. Langmuir 30:5455–5459

Son Y, Kim C (2009) Spreading of inkjet droplet of non-Newtonian fluid on solid surface with controlled contact angle at low Weber and Reynolds numbers. J Non-Newton Fluid Mech 162:78–87

Tirtaatmadja V, McKinley GH, Cooper-White JJ (2006) Drop formation and breakup of low viscosity elastic fluids: effects of molecular weight and concentration. Phys Fluids 18:043101

Tran T et al (2013) Droplet impact on superheated micro-structured surfaces. Soft Matter 9:3272–3282

Ukiwe C, Kwok DY (2005) On the maximum spreading diameter of impacting droplets on well-prepared solid surfaces. Langmuir 21:666–673